Dalton Transactions

PAPER

View Article Online
View Journal | View Issue

Cite this: *Dalton Trans.*, 2026, **55**, 2635

A family of thienyl-bis-salophen Zn(II) complexes for enhancing photoconductance in hybrid materials including platinum ultra-small nanoparticles

Melissa Dumartin,[a] Adeline Pham,[b] Nathalie Saffon-Merceron,[c] Marine Tassé,[d] Simon Tricard,[b] Claire Kammerer[a] and Jacques Bonvoisin *[a]

Received 12th November 2025,
Accepted 8th January 2026

DOI: 10.1039/d5dt02712h

rsc.li/dalton

The design, synthesis and characterization of a series of thienyl-substituted bis-salophen ligands and their related dinuclear Zn(II) complexes are reported, as multifunctional platforms combining the presence of metal centers, multiple free coordinating sites and solubilizing groups. Some of these molecules have been successfully used to elaborate hybrid materials through self-assembly with ultra-small platinum nanoparticles. Interaction of the bis-salophen Zn(II) complexes with the nanoparticles, mediated by the thiophene coordinating moieties, led to a significant enhancement of the photoconductance properties.

Introduction

Hybrid materials made of assemblies of nanoparticles can show specific electrical properties that depend on the nature and the organization of the building blocks.[1,2] Charge transport in these systems is obviously influenced by the nanoparticles, but can also be controlled by a strategic choice of functional molecules inserted into the structure.[3] When using ultra-small nanoparticles, Coulomb blockade is present at room temperature. We demonstrated that molecular effects are of primary importance and that a determining parameter is the polarizability of the molecules.[4,5] Thus, a fine control of the structure of the molecules can provide functional diversity for the use of such materials in electrical and electronic engineering. Indeed, well-defined organic synthesis strategies have already enabled fundamental studies in the field of molecular electronics.[6,7] In hybrid materials including nanoparticles, we observed that the nature of the interaction between the functional groups of the molecules and the nanoparticle surface can influence the nanostructuration of the materials, and their electrical response.[8,9] Designing appropriate coordination groups is thus decisive. Recently, we showed that coordination bonds between molecular entities and the surface of inorganic nanoparticles can be an efficient tool to tune photoconductance.[10] In that study, we demonstrated that the number of pyridines present on a zinc porphyrin scaffold drastically reinforced both the structural cohesion of the system and its photoconductive response. On the other hand, as the organization at the nanoscale occurs in solution, before the shaping of the materials, it is crucial to consider the solubility of the molecular building blocks in the same solvent as the nanoparticles, *i.e.*, THF in our case.[5,10] The goal of the present study is thus to develop the synthesis of molecular complexes, which will form nanostructured hybrid materials with Pt nanoparticles and enhance the photoconductance properties of the obtained systems. The first aim of this work is to synthesize a molecular platform that fulfills the following three parameters: (1) the possibility to introduce metal atoms and give rise to coordination complexes, as a way to tune molecular polarizability – especially as in such structures the two metal centers can interact electronically with each other, (2) the possibility to incorporate solubilizing groups, to adjust the solubility of such molecules in organic solvents, and (3) the presence of multiple free coordination sites in the molecular scaffold, to bridge the nanoparticles and ensure cohesion of the hybrid system. Once these molecular building blocks are in hand, the second goal of this study is to synthesize the hybrid materials including Pt nanoparticles and study their response in photoconductance.

Bis-salophens were selected as platform molecules, as they are readily accessible compounds, allow straightforward functionalization of their scaffold, and exhibit attractive structural properties. In addition, bis-salophens are versatile ligands that have attracted growing interest in the field of

[a]*CEMES, CNRS-UPR 8011, Université de Toulouse, 29 rue Jeanne Marvig, 31055 Toulouse, France. E-mail: jacques.bonvoisin@cemes.fr*
[b]*Laboratoire de Physique et Chimie des Nano-Objets, INSA, CNRS-UMR5215, Université de Toulouse, 135 Avenue de Rangueil, 31077 Toulouse, France*
[c]*Université de Toulouse, Institut de Chimie de Toulouse, ICT UAR 2599, 118 route de Narbonne, 31062 Toulouse, France*
[d]*Laboratoire de Chimie de Coordination, CNRS-UPR8241, Université de Toulouse, 205 route de Narbonne, 31077 Toulouse, France*

coordination chemistry, thanks in particular to the groundbreaking work of A. W. Kleij.[11–15] Their specific structure gives rise to unique properties that enable them to form stable complexes with various metals, opening the way to a wide range of applications in catalysis,[16,17] electrochemistry[14,18] and synthesis of new functional materials.[19–22] In particular, considering electrical measurements, the planar conformation of bis-salophen molecules makes them ideal platforms for physisorption on surfaces, forming ordered self-assembled structures addressable by STM measurements. However, only a few reports can be found on STM studies of bis-salophen complexes,[11] whereas most of the STM investigations focus on salophen itself.[23–29] In this context, we recently reported the synthesis and characterization of iodo-substituted bis-salophen complexes as molecular building blocks for the elaboration of complicated self-assembled halogen-bonded nanoarchitectures.[30]

In the framework of the present study, the design of bis-salophen candidates to be inserted into hybrid materials was adjusted according to the specifications given above. First, regarding the possible insertion of metal atoms, the Zn(II) cation was selected for the formation of coordination complexes, owing to its diamagnetic character which simplifies characterization studies (in particular, through the use of conventional NMR). Next, given the natural tendency of the flat bis-salophens to aggregate by π-stacking, *tert*-butyl groups were appended in order to increase the solubility of such molecular platforms in solvents compatible with the chemistry of ultra-small nanoparticles, namely, tetrahydrofuran. Finally, coordinating groups were inserted around the bis-salophen scaffold to promote interactions with the nanoparticles. When molecular systems are planned to interact with noble metals such as gold or platinum, thiols are generally preferred. However, in assemblies with ultra-small nanoparticles, we usually opt for weaker coordination groups in order to obtain larger organization by facilitating trial-and-error mechanisms and to avoid self-coordination of the molecular platforms. Thiophene was, for instance, demonstrated to be a moiety of choice for elaborating nanostructured hybrid materials combining iron-based coordination polymers and platinum nanoparticles.[31] According to these specifications, a series of six target bis-salophen Zn(II) complexes were thus designed (Fig. 1), incorporating either 3-thiophene or 2-thiophene substituents *ortho* (**16**, **18**) or *para* (**3**, **5**, **9**, **13**) with regard to the oxygen atoms, so as to vary the position of the sulfur coordination sites within the scaffold and thus modulate interactions with the nanoparticles. Potential solubility issues were addressed by inserting *t*Bu groups into four of the target complexes, either *ortho* (**9**, **13**) or *para* (**16**, **18**) to the oxygen atoms. Finally, in order to probe the influence of coordinated metal atoms on the properties of hybrid assemblies, two non-metallated bis-salophen targets were also devised, incorporating *t*Bu groups *ortho* to the hydroxyl moieties and 3- or 2-thiophenes at the *para* positions (compounds **8** and **12**, respectively).

Herein, we report the synthesis and characterization of a new series of thienyl-substituted bis-salophens and their related Zn(II) complexes. The formation of hybrid materials through self-assembly of some of these multifunctional molecules with ultra-small platinum nanoparticles in THF solution is then presented, along with an evaluation of their photoconductive properties.

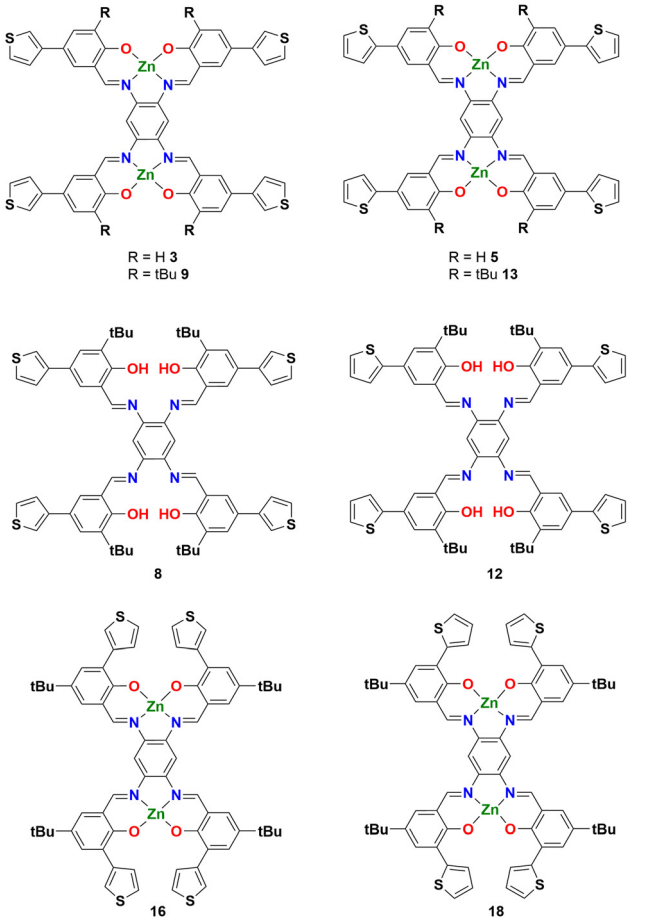

Fig. 1 Structures of the thienyl-bis-salophen Zn(II) complexes (**3**, **5**, **9**, **13**, **16**, **18**) and free ligands (**8**, **12**) studied in this work.

Results and discussion

Synthesis of the thienyl-substituted bis-salophen target compounds

According to a general synthetic route, bis-salophen Zn(II) complexes were obtained from the corresponding thiophene-substituted 2-hydroxybenzaldehyde, 1,2,4,5-benzenetetramine hydrochloride and zinc(II) diacetate in one step (for targets **3**, **5**, **16** and **18**) or two steps (for **9** and **13**). In the latter case, the free ligands **8** and **12**, respectively, were isolated before coordination to Zn(II). As already mentioned in previous works,[30,32] the use of polar solvents such as DMSO or MeOH is essential in these syntheses in order to isolate the desired bis-salophens in good yields.

The target Zn(II) complexes lacking *t*Bu solubilizing groups were synthesized first. Bis-salophen **3**, bearing 3-thiophene groups at the *para* position with regard to the oxygens, was

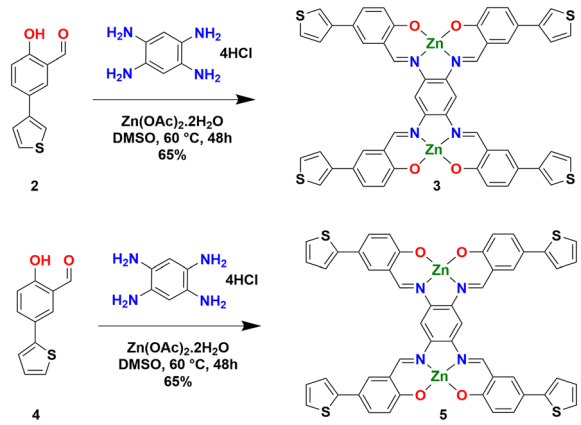

Scheme 1 One-step synthesis of bis-salophen Zn(II) complexes **3** and **5**.

obtained in one step from 2-hydroxybenzaldehyde precursor **2**, bearing a 3-thiophene at position 5 (Scheme 1).[33,34] The formation of the tetra-imine in the presence of 1,2,4,5-benzenetetramine and coordination to Zn(II) were carried out in a single pot in the presence of zinc diacetate. After 48 h at 60 °C in DMSO, the desired complex **3** was obtained in 65% yield. Following the same strategy, 2-thiophene-substituted benzaldehyde **4**[35] successfully yielded bis-salophen complex **5**.

Analogues of complexes **3** and **5** bearing *t*Bu solubilizing groups were then devised, keeping the 3- and 2-thiophene substituents at the same positions. The synthesis of the resulting complexes **9** and **13** started with the preparation of the appropriately substituted benzaldehyde precursors **7** and **11**, respectively (Scheme 2). The latter were both obtained from 3-(*tert*-butyl)-2-hydroxy-5-iodobenzaldehyde (**6**),[36] which underwent cross-couplings to install the thiophene moiety at position 5. A Suzuki–Miyaura coupling with 3-thienylboronic acid afforded the key precursor **7** in 80% yield, whereas a Stille cross-coupling involving 2-(tributylstannyl)thiophene gave rise to benzaldehyde **11**. Two further steps were then required to obtain the target Zn(II) complexes **9** and **13**. *t*Bu-appended benzaldehydes **7** and **11** were first reacted with 1,2,4,5-benzenetetramine in methanol at room temperature to give the tetra Schiff bases **8** and **12** in 85% and 65% yields, respectively. As tentative target molecules for hybrid assemblies, these free ligands were isolated and fully characterized by NMR, HRMS and XRD (see below). In parallel, zinc coordination was successfully achieved for the 3- and 2-thiophene-appended bis-salophens, in the presence of $Zn(OAc)_2$ in methanol, thus affording target complexes **9** and **13** in 85% and 95% yields, respectively.

In order to vary the position of the thiophene groups within the bis-salophen scaffold and thus modulate the properties of the resulting hybrid materials, permutation of the thiophene and *t*Bu moieties was envisioned, *i.e.*, positioning the thiophenes *ortho* and the *t*Bu *para* with regard to the oxygens. The resulting Zn(II) complex **16**, bearing a 3-thiophene group at the *ortho* position, was obtained in two steps from 5-(*tert*-butyl)-2-hydroxy-3-iodobenzaldehyde (**14**)[37] (Scheme 3). The latter was engaged in a Suzuki–Miyaura cross-coupling reaction with 3-thienylboronic acid, thus affording the functionalized building block **15**. Bis-salophen Zn(II) complex **16** was then obtained in a single step in 80% yield by condensation of 1,2,4,5-benzenetetramine and benzaldehyde **15** in the presence of zinc diacetate. Finally, the isomer **18**, bearing a 2-thiophene group at the *ortho* position, was prepared from hydroxybenzaldehyde **14** according to a similar synthetic route, involving a Stille cross-coupling followed by a condensation in the presence of the zinc(II) salt. Importantly, many attempts were made to obtain free bis-salophen ligands prior to the synthesis of complexes **16** and **18**, but they were unsuccessful.

This series of target molecules, including two free ligands (**8** and **12**) and six bis-salophen Zn(II) complexes (**3**, **5**, **9**, **13**, **16** and **18**), was thus successfully synthesized and subsequently characterized by NMR spectroscopy, HRMS and elemental analysis (for the Zn(II) complexes). It is important to note that the Zn(II) complexes having the thiophene moiety located *para* to the oxygen atom exhibited low solubility in organic solvents, regardless of the presence (**9** and **13**) or absence (**3** and **5**) of *tert*-butyl substituents. In such cases, the NMR spectra were recorded in a mixture of DMSO-d_6 and tetrabutylammonium acetate (TBA acetate), as the acetate anion presumably prevents π-stacking by coordinating to the zinc atoms, thus increasing the solubility of the complexes.

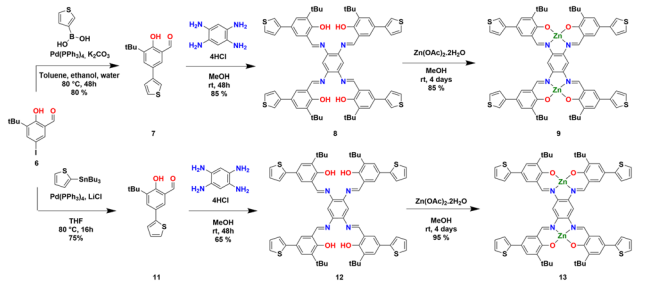

Scheme 2 Synthesis of the free bis-salophen ligands **8** and **12** and of the related Zn(II) complexes **9** and **13**.

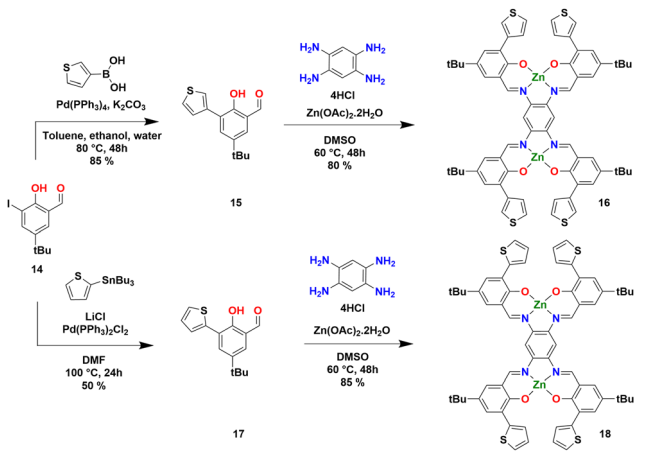

Scheme 3 Synthesis of bis-salophen Zn(II) complexes **16** and **18**.

X-ray diffraction analysis

The two free ligands **8** and **12** and three bis-salophen Zn(II) complexes (**13**, **16** and **18**) were crystallized and their structures were determined by single-crystal X-ray diffraction (Fig. 2 and S34; Tables S1–S4 in the SI). The structures of the two ligands are different from each other: tetra-Schiff base **8** crystallizes in a centrosymmetric space group with the symmetry center located at the middle of the central benzene ring. The asymmetric unit contains one half of the molecule and a solvent molecule, making the molecule perfectly symmetrical. Ligand **12** also crystallizes in a centrosymmetric space group, but its asymmetric unit contains the whole molecule and three solvent molecules. In both structures, the OH hydrogen atoms of the phenol groups are involved in intramolecular hydrogen-bonding interactions with the N atoms of the imine groups (Fig. S35, Tables S5 and S6 *cf* the SI). The salicylidene units are not coplanar with the central benzene ring, and the distortion from planarity can be described by the C═C–N═C imine torsional angles (16.6° and 53.5° for tetra-Schiff base **8**, and a 33.8–38.2° range for **12**, see Table S4 in the SI).[37] All the three bis-salophen Zn(II) complexes **13**, **16** and **18** crystallize in centrosymmetric space groups and their asymmetric units contain one half of the dinuclear Zn(II) complex, making each complex perfectly symmetrical. In the three structures, both Zn metal centers are bonded to the O of the solvent molecule (DMSO or acetone), which are positioned in an *anti*-fashion with respect to the salophen framework. The structures of complexes **16** and **18** are isostructural in the trigonal $R\bar{3}$ space group. In each complex, the coordination geometry can be viewed as a distorted five-coordinate square pyramid, as it is already known for such structures[38–40] with τ_5 values between 0.04 (**16** and **18**) and 0.18 (**13**). The axial site is occupied by the Zn atom; its deviation from the mean plane defined by O1, O2, N1 and N2 is 0.23 Å (**13**) and 0.39 Å (**16** and **18**). The Zn–O and Zn–N distances (Zn1–O1, Zn1–O2, Zn1–N1 and Zn1–N2) found within the three complexes are in the range of distances reported for other bis-salophen Zn(II) complexes.[32,41,42] If we compare the bond lengths within the three complexes studied in this work, the bis-salophen Zn(II) complex **13** bearing a 2-thiophene group at the *para* position with regard to the oxygen exhibits the shortest Zn–O and Zn–N bond lengths (and the longest metal–solvent Zn–O3 bond), whereas isomer **18**, bearing the 2-thiophene groups at the *ortho* position, exhibits the longest Zn–O and Zn–N bond lengths (and the shortest metal–solvent Zn–O3 bond). In all three complexes, the metal–solvent Zn–O3 bond distance is slightly elongated compared to the Zn–O1 and Zn–O2 bond distances (see Table S2 in the SI). As in the free ligands **8** and **12**, the salicylidene units in Zn(II) complexes **13**, **16** and **18** are not coplanar with the central benzene ring, but the distortion from planarity as measured by the C═C–N═C imine torsional angles is smaller (2.3° and 10.9° for **13**, 12.1° and 25.3° for **16**, and 14.7° and 22.5° for **18**, see Table S4 in the SI).

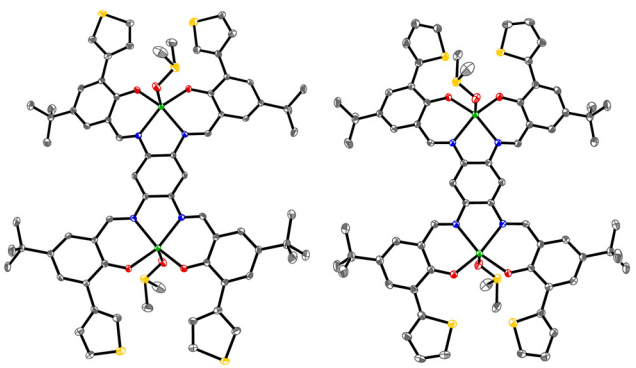

Fig. 2 Molecular views of complexes **16** (left) and **18** (right). Thermal ellipsoids are drawn at the 30% probability level. H atoms, disordered atoms and solvent molecules are omitted for clarity.

Synthesis of the hybrid materials

Once the molecular platforms were in hand and unambiguously characterized, the synthesis of the hybrid materials was undertaken. First, Pt nanoparticles were synthesized by decomposition of $Pt_2(dba)_3$ (dba = dibenzylideneacetone) under a carbon monoxide (CO) atmosphere in THF, followed by washing of the organic dba ligands with pentane, as previously reported.[4,5,8,10,31] After washing, the nanoparticles were dispersed in THF. This protocol allows obtaining "naked" ultra-small Pt nanoparticles (called **Pt NP**) without any organics, stabilized by CO and THF, with a mean size of 1.4 nm (Fig. S1 in the SI). As stated previously, the question of solubility of the molecular compounds in THF is crucial for the self-assembly step. We did not find any way to solubilize the bis-salophen Zn(II) complexes **3** and **5** in THF in the absence of the solubilizing *t*Bu moieties. Even complexes **9** and **13**, with the *t*Bu groups located *ortho* to the oxygen, were hard to solubilize, as mentioned earlier. It was then necessary to add tetrabutylammonium acetate (or bromide) to decrease intermolecular interactions and make the complexes slightly soluble.[30,32] Unfortunately, the presence of acetate brought a strong competition with the complexes of interest during the self-assembly process, as the carboxylate groups interacted with the platinum surface. We thus did not consider complexes **9** and **13** for the formation of the hybrid materials and focused our attention on compounds **16** and **18**, which are soluble enough in THF without any additives. The grafting of the *t*Bu moieties *para* to the oxygens of the bis-salophen was thus a successful strategy to circumvent the solubility issue. The hybrid materials were prepared by self-assembly, by mixing THF solutions of **Pt NP** and of molecule **16** or **18**, respectively, and stirring the resulting mixture for two hours. The relative amount of each solution was adjusted to achieve a bis-salophen/Pt ratio of 0.05 equivalents (corresponding to ~5 bis-salophen ligands per nanoparticle and to 20 equivalents of Pt atoms per bis-salophen ligand). We obtained two hybrid materials called **SA-16** and **SA-18**. In both of them, the Zn : Pt ratio measured by scanning electron microscopy coupled with energy-dispersive X-ray spectroscopy was in good agreement with the expected bis-salophen/Pt ratio of 0.05 equivalents (Fig. S2 in the SI).

Transmission electron microscopy (TEM) showed that submicron rod-shaped assemblies were formed, without any significant morphological differences between the two systems (Fig. 3a and c). Each assembly was constituted by an aggregation of the Pt nanoparticles associated with the bis-salophens (Fig. 3b and d). No specific long-range ordering was observed by TEM within the aggregates. However, small-angle X-ray scattering (SAXS) proved the presence of local order in the assemblies, as broad peaks were observed in the q-range of 0.28 $Å^{-1}$, which corresponds to a specific correlation distance between the nanoparticles estimated to be 2.3 nm (Fig. S3 in the SI). The size of the nanoparticles being equal to 1.4 nm, the edge-to-edge distance between two nanoparticles is thus equal to 0.9 nm on average. The size of the functionalized bis-salophen Zn(II) complexes is *ca.* 1.6 nm for **16** and 2 nm for **18** (from one edge of a thiophene to the other), as seen in X-ray crystal structures. We thus expect that the molecules separated the nanoparticles in an anisotropic way, with a "face-on" bonding mode through metal–π interactions, in addition to the coordination between the thiophene moieties and the Pt surface of other nanoparticles.

Fourier-transform infrared spectroscopy was performed to prove the coordination of the bis-salophens to the surface of the nanoparticles (Fig. 4). The vibration of the CO bonded in a terminal mode to the Pt surface was observed at 2039 cm^{-1} in the ligand-free "naked" nanoparticles. The shift of this vibration to 2043 cm^{-1} in **SA-16** and to 2042 cm^{-1} in **SA-18** meant that the electron density at the surface changed because of ligand coordination.[43] Such higher wavenumbers corresponded to a depletion of electron density at the surface. Indeed, lower electron density at the surface implies weaker back-donation from the nanoparticles to the antibonding orbitals of the CO molecule, leading to the appearance of a vibration band at a higher wavenumber. The creation of coordination bonds between the thiophene moieties and the Pt surface thus allowed electronic communication between these two entities in the hybrid materials.

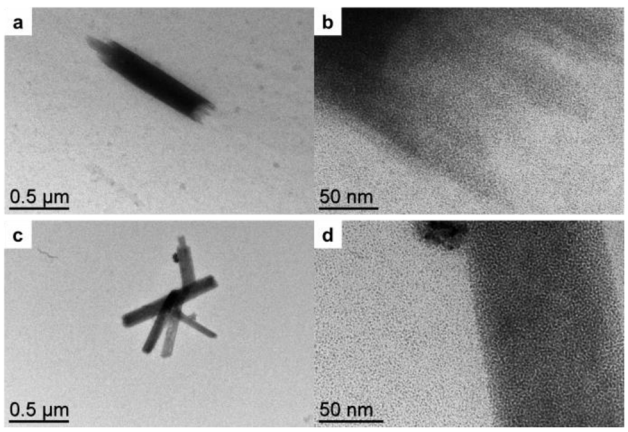

Fig. 3 TEM pictures of the self-assemblies of **Pt NP** with bis-salophen Zn(II) complexes **16** and **18**. (a and b) **SA-16** and (c and d) **SA-18**. (b) and (d) are zoomed-in views of (a) and (c), respectively.

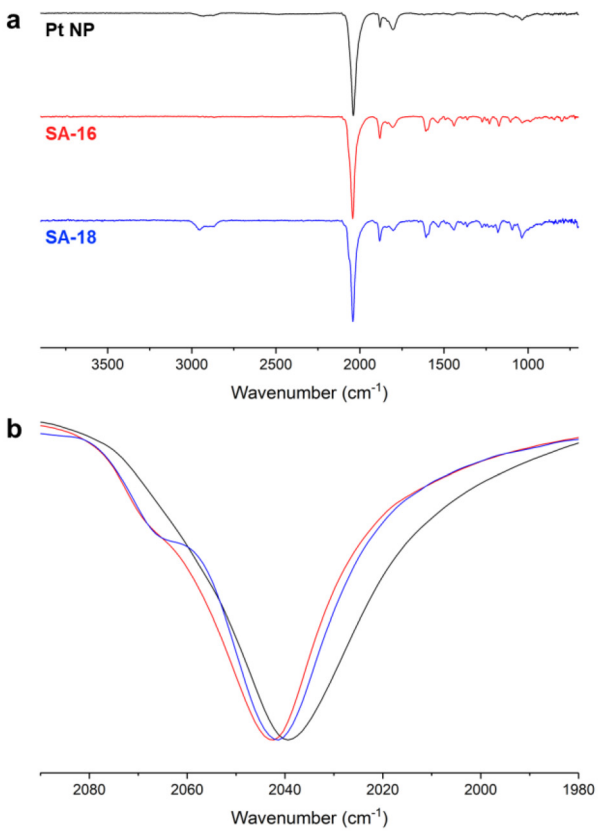

Fig. 4 Infrared spectra of the pristine **Pt NP** and of the **SA-16** and **SA-18** self-assemblies: (a) full spectra and (b) zoomed-in view of the terminal CO region; peak maxima: **Pt NP**: 2039 cm^{-1}, **SA-16**: 2043 cm^{-1} and **SA-18**: 2042 cm^{-1}.

(Photo)electrical properties

To study further the electronic communication, charge-transport measurements were performed by conductive atomic force microscopy (CAFM), coupled to statistical analyses. The assemblies were drop-cast onto a gold surface, and a large number of *I–V* curves (~50) were obtained by connecting the CAFM tip at different positions of individual objects. The *I–V* curves were normalized at 2 V and averaged to compare the current characteristics of one sample with another (Fig. 5a). The nonlinear behavior of the *I–V* curves results from the presence of Coulomb blockade at room temperature. The non-linearity of the curves significantly increased in the presence of bis-salophen Zn(II) complexes compared to assemblies of "naked" Pt nanoparticles. Coulomb blockade comes from the charging energy E_C of a nanoparticle, defined as $E_C = e^2/(2\pi\varepsilon_r\varepsilon_0 d \ln(s/(s-d)))$, where e is the charge of the electron, ε_0 is the permittivity of vacuum, ε_r is the dielectric constant of the medium surrounding the particles, d is the particle diameter, and s is the center-to-center distance between two particles. The observation of a strong similar non-linearity in the *I–V* characteristics of **SA-16** and **SA-18** comes from the fact that s, d and ε_r are comparable in both systems. Here, we confirm

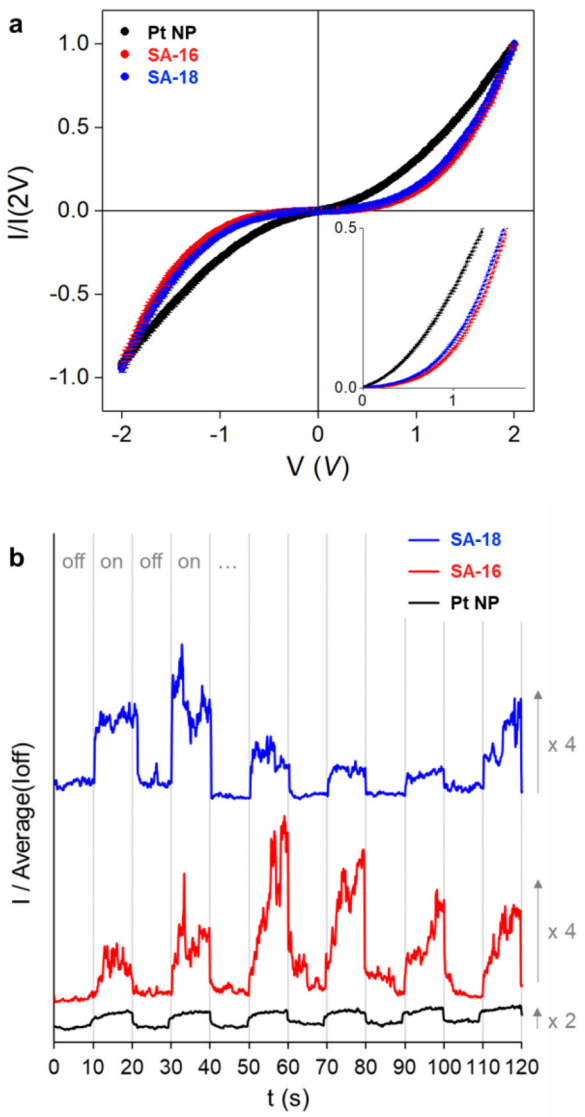

Fig. 5 Charge transport measurements at the nanoscale, performed by conductive AFM on **Pt NP**, **SA-16**, and **SA-18**, at room temperature. (a) *I–V* curves; the curves are normalized at 2 V; inset: magnification of the 0–1.5 V region. (b) Evolution of the current intensity under light irradiation at a voltage of 2 V; light is successively switched on and off.

that choosing large, rigid molecules with specific coordination groups is an effective strategy for improving Coulomb blockade, as it drives large interparticle distances.[10]

Photoconductance measurements were carried out by focusing a laser on the assemblies at the interface between the AFM tip and the substrate. On–off photoconductivity tests have been conducted using light with a wavelength of 532 nm in the main absorption bands of the bis-salophens (Fig. S4 in the SI), and a power of 10 mW revealed a fourfold increase in current for **SA-16** and **SA-18** under illumination, whereas it was only a twofold increase for the reference **Pt NP** (Fig. 5b). Although local heating effects or nanoparticle polarization cannot be completely ruled out, these results demonstrate a clear enhancement in photoconduction when bis-salophen antennas are used. This enhancement is likely linked to the dynamic quenching mechanism, which promotes energy transfer from the molecules to the nanoparticles under light exposure.[10] Additionally, irradiation may increase the polarizability of the molecules, as the excited-state redistribution of electron density leads to a greater population of antibonding orbitals. As in the example using functionalized porphyrins, significant current fluctuations were observed over time. These fluctuations are characteristic of percolation-based charge transport in granular systems formed by nanoparticle aggregates and were significantly enhanced under light irradiation.

Conclusions

In summary, we synthesized and characterized a new series of thienyl-substituted bis-salophens and their related Zn(II) dinuclear complexes, as multifunctional platform molecules incorporating metal centers, free coordinating sites, and solubilizing groups. Two of the Zn(II) complexes enabled the formation of hybrid materials through self-assembly with ultrasmall platinum nanoparticles in THF. Coordination of the complexes to the nanoparticles, mediated by thiophene units, resulted in a marked improvement in photoconductive properties. However, the position of the sulfur atoms, either axial (in the 3-thiophene derivative) or lateral (in the 2-thiophene derivative), did not lead to significant differences both in the structuring of the materials and in their (photo)electrical response. Nonetheless, this study confirms the effectiveness of the addition of coordinating groups to the molecular design strategy for enhancing optoelectronic performance in nanostructured hybrid systems. An advantage of coordination chemistry is the possibility of exchanging the metal centers, which could influence charge transport mechanisms in hybrid materials. Furthermore, as a perspective, the synthesis of bimetallic bis-salophens would allow dissymmetric compounds to be obtained and thus an induced local polarization of the charge density near the surface of the nanoparticles.

Author contributions

S. T., C. K. and J. B. performed the conceptualization, supervision and funding acquisition; M. D. carried out all the chemical synthesis and the characterization studies of the bis-salophen series; A. P. and M. T. performed the synthesis of the hybrid materials and the photoelectrical measurements; N. S.-M. conducted the X-ray diffraction analysis; S. T., C. K. and J. B. directed the research and wrote the manuscript; and all the authors discussed and commented on the manuscript.

Conflicts of interest

There are no conflicts to declare.

Data availability

Supplementary information (SI): figures, synthetic procedures, characterization of chemical compounds (NMR spectra of synthetic intermediates and targets) and hybrid materials. See DOI: https://doi.org/10.1039/d5dt02712h.

CCDC 2404730 (**8**), 2404731 (**12**), 2404732 (**13**), 2404733 (**16**) and 2404734 (**18**) contain the supplementary crystallographic data for this paper.[44a–e]

Acknowledgements

Financial support from the Agence Nationale de la Recherche (DINAPO grant ANR-23-CE09-0006-02, and MOMA grant ANR-23-ERCC-0008-01) is acknowledged. This study has been partially supported through the EUR grant NanoX no. ANR-17-EURE-0009 (THERESA project) in the framework of the Programme des Investissements d'Avenir. This work was also supported by the CNRS and the Université de Toulouse. Technical assistance provided by the Institut de Chimie de Toulouse (ICT-UAR 2599) and by the Centre de Microcaractérisation Raimond Castaing (UAR 3623) is gratefully acknowledged.

References

1 A. Zabet-Khosousi and A. A. Dhirani, *Chem. Rev.*, 2008, **108**, 4072–4124.
2 D. V. Talapin, J. S. Lee, M. V. Kovalenko and E. V. Shevchenko, *Chem. Rev.*, 2010, **110**, 389–458.
3 J. H. Liao, S. Blok, S. J. van der Molen, S. Diefenbach, A. W. Holleitner, C. Schonenberger, A. Vladyka and M. Calame, *Chem. Soc. Rev.*, 2015, **44**, 999–1014.
4 A. Gillet, S. Cher, M. Tasse, T. Blon, S. Alves, G. Izzet, B. Chaudret, A. Proust, P. Demont, F. Volatron and S. Tricard, *Nanoscale Horiz.*, 2021, **6**, 271–276.
5 S. Tricard, O. Said-Aizpuru, D. Bouzouita, S. Usmani, A. Gillet, M. Tasse, R. Poteau, G. Viau, P. Demont, J. Carrey and B. Chaudret, *Mater. Horiz.*, 2017, **4**, 487–492.
6 A. K. Flatt, S. M. Dirk, J. C. Henderson, D. E. Shen, J. Su, M. A. Reed and J. M. Tour, *Tetrahedron*, 2003, **59**, 8555–8570.
7 N. Stuhr-Hansen, J. K. Sorensen, K. Moth-Poulsen, J. B. Christensen, T. Bjornholm and M. B. Nielsen, *Tetrahedron*, 2005, **61**, 12288–12295.
8 G. Manai, H. Houimel, M. Rigoulet, A. Gillet, P. F. Fazzini, A. Ibarra, S. Balor, P. Roblin, J. Esvan, Y. Coppel, B. Chaudret, C. Bonduelle and S. Tricard, *Nat. Commun.*, 2020, **11**, 2051.
9 L. Merle, G. Manai, A. Pham, S. Lecommandoux, P. Demont, C. Bonduelle, S. Tricard, A. Mlayah and J. Grisolia, *J. Phys. Chem. C*, 2021, **125**, 22643–22649.
10 N. Marchenko, D. Martin, A. Pham, S. Abid, E. Cretal, A. Ibarra, D. Lagarde, M. Tassé, J. Bonvoisin, G. Rapenne, J. Grisolia, C. Kammerer and S. Tricard, *Mater. Horiz.*, 2025, **12**, 3429–3435.
11 G. Salassa, M. J. J. Coenen, S. J. Wezenberg, B. L. M. Hendriksen, S. Speller, J. Elemans and A. W. Kleij, *J. Am. Chem. Soc.*, 2012, **134**, 7186–7192.
12 S. J. Wezenberg, E. C. Escudero-Adan, J. Benet-Buchholz and A. W. Kleij, *Inorg. Chem.*, 2008, **47**, 2925–2927.
13 S. J. Wezenberg and A. W. Kleij, *Angew. Chem., Int. Ed.*, 2008, **47**, 2354–2364.
14 C. J. Whiteoak, G. Salassa and A. W. Kleij, *Chem. Soc. Rev.*, 2012, **41**, 622–631.
15 A. W. Kleij, *Dalton Trans.*, 2009, 4635–4639.
16 I. Jacobs, A. C. T. van Duin, A. W. Kleij, M. Kuil, D. M. Tooke, A. L. Spek and J. N. H. Reek, *Catal. Sci. Technol.*, 2013, **3**, 1955–1963.
17 M. Kuil, P. E. Goudriaan, A. W. Kleij, D. M. Tooke, A. L. Spek, P. van Leeuwen and J. N. H. Reek, *Dalton Trans.*, 2007, 2311–2320.
18 J. C. Wu, S. X. Liu, T. D. Keene, A. Neels, V. Mereacre, A. K. Powell and S. Decurtins, *Inorg. Chem.*, 2008, **47**, 3452–3459.
19 R. M. Clarke and T. Storr, *Dalton Trans.*, 2014, **43**, 9380–9391.
20 J. Zhao, F. F. Dang, B. Liu, Y. Wu, X. L. Yang, G. J. Zhou, Z. X. Wu and W. Y. Wong, *Dalton Trans.*, 2017, **46**, 6098–6110.
21 S. M. Ebert and M. Mastalerz, *Org. Mater.*, 2020, **2**, 182–203.
22 A. K. Crane and M. J. MacLachlan, *Eur. J. Inorg. Chem.*, 2012, 17–30.
23 A. DiLullo, S. H. Chang, N. Baadji, K. Clark, J. P. Klockner, M. H. Prosenc, S. Sanvito, R. Wiesendanger, G. Hoffmann and S. W. Hla, *Nano Lett.*, 2012, **12**, 3174–3179.
24 M. T. Raisanen, F. Mogele, S. Feodorow, B. Rieger, U. Ziener, M. Leskela and T. Repo, *Eur. J. Inorg. Chem.*, 2007, 4028–4034.
25 M. Viciano-Chumillas, D. Z. Li, A. Smogunov, S. Latil, Y. J. Dappe, C. Barreteau, T. Mallah and F. Silly, *Chem. – Eur. J.*, 2014, **20**, 13566–13575.
26 Y. C. Zhang, B. Chilukuri, T. B. Hanson, Z. M. Heiden and D. Y. Lee, *J. Phys. Chem. Lett.*, 2019, **10**, 3525–3530.
27 E. Sierda, M. Abadia, J. Brede, M. Elsebach, B. Bugenhagen, M. H. Prosenc, M. Bazarnik and R. Wiesendanger, *ACS Nano*, 2017, **11**, 9200–9206.
28 L. Mengozzi, M. El Garah, A. Gualandi, M. Iurlo, A. Fiorani, A. Ciesielski, M. Marcaccio, F. Paolucci, P. Samori and P. G. Cozzi, *Chem. – Eur. J.*, 2018, **24**, 11954–11960.
29 J. Elemans, S. J. Wezenberg, M. J. J. Coenen, E. C. Escudero-Adán, J. Benet-Buchholz, D. den Boer, S. Speller, A. W. Kleij and S. De Feyter, *Chem. Commun.*, 2010, **46**, 2548–2550.
30 M. Lacaze, N. Saffon-Merceron, F. Silly and J. Bonvoisin, *J. Mol. Struct.*, 2021, **1223**, 129319.
31 S. Usmani, M. Mikolasek, A. Gillet, J. S. Costa, M. Rigoulet, B. Chaudret, A. Bousseksou, B. Lassalle-Kaiser, P. Demont, G. Molnar, L. Salmon, J. Carrey and S. Tricard, *Nanoscale*, 2020, **12**, 8180–8187.

32 E. C. Escudero-Adan, M. M. Belmonte, E. Martin, G. Salassa, J. Benet-Buchholz and A. W. Kleij, *J. Org. Chem.*, 2011, **76**, 5404–5412.
33 V. Ramakrishna and N. D. Reddy, *Dalton Trans.*, 2017, **46**, 8598–8610.
34 V. Gupta, D. Sahu, S. Jain, K. Vanka and R. P. Singh, *Org. Biomol. Chem.*, 2019, **17**, 8853–8857.
35 E. Lindback, H. Norouzi-Arasi, E. Sheibani, D. Y. Ma, S. Dawaigher and K. Warnmark, *ChemistrySelect*, 2016, **1**, 1789–1794.
36 A. Promchat, P. Rashatasakhon and M. Sukwattanasinitt, *J. Hazard. Mater.*, 2017, **329**, 255–261.
37 R. Schnorr, M. Handke and B. Kersting, *Z. Naturforsch., B:J. Chem. Sci.*, 2015, **70**, 757–763.
38 A. W. Addison, T. N. Rao, J. Reedijk, J. Vanrijn and G. C. Verschoor, *J. Chem. Soc., Dalton Trans.*, 1984, 1349–1356.
39 M. Enamullah, A. Uddin, G. Pescitelli, R. Berardozzi, G. Makhloufi, V. Vasylyeva, A. C. Chamayou and C. Janiak, *Dalton Trans.*, 2014, **43**, 3313–3329.
40 L. Yang, D. R. Powell and R. P. Houser, *Dalton Trans.*, 2007, 955–964.
41 D. Anselmo, G. Salassa, E. C. Escudero-Adan, E. Martin and A. W. Kleij, *Dalton Trans.*, 2013, **42**, 7962–7970.
42 S. J. Wezenberg, D. Anselmo, E. C. Escudero-Adan, J. Benet-Buchholz and A. W. Kleij, *Eur. J. Inorg. Chem.*, 2010, 4611–4616.
43 C. Dablemont, P. Lang, C. Mangeney, J. Y. Piquemal, V. Petkov, F. Herbst and G. Viau, *Langmuir*, 2008, **24**, 5832–5841.
44 (*a*) CCDC 2404730: Experimental Crystal Structure Determination, 2026, DOI: 10.5517/ccdc.csd.cc2lq9yl; (*b*) CCDC 2404731: Experimental Crystal Structure Determination, 2026, DOI: 10.5517/ccdc.csd.cc2lq9zm; (*c*) CCDC 2404732: Experimental Crystal Structure Determination, 2026, DOI: 10.5517/ccdc.csd.cc2lqb0p; (*d*) CCDC 2404733: Experimental Crystal Structure Determination, 2026, DOI: 10.5517/ccdc.csd.cc2lqb1q; (*e*) CCDC 2404734: Experimental Crystal Structure Determination, 2026, DOI: 10.5517/ccdc.csd.cc2lqb2r.